Communication and Power Transfer Analysis of Interfering Magnetically Resonant Coupled Systems

Richard Fischbacher, *Student Member, IEEE*, Jose Romero Lopera, *Student Member, IEEE*, David Pommerenke, *Fellow, IEEE*, Ralph Prestros, *Member, IEEE*, Bernhard Auinger, *Member, IEEE*, Wolfgang Bösch, *Fellow, IEEE*, and Jasmin Grosinger, *Senior Member, IEEE*

***Abstract*—This work presents, for the first time, a communication and power transfer analysis of interfering wireless power transfer (WPT) and near-field communication (NFC) systems. The communication analysis is conducted by investigating the NFC tag-to-reader communication quality in the digital baseband while being interfered with by WPT. The power transfer analysis is conducted by investigating the maximum power transferred and WPT efficiency η while being affected by the passive loading effects of the NFC prototype system. Inductive decoupling techniques are applied to improve the communication quality and WPT performance. Good communication quality was achieved with at least 60 % inductive decoupling. A system-level adjustment of the communication signal demodulation achieved further communication quality improvements, requiring only 15 % inductive decoupling. The WPT performance was improved by inductive decoupling, shown by an improved maximum power transfer of up to 27 % and an improved WPT efficiency η from 0.42 to 0.67. Additionally, inductive decoupling reduced the chance of the WPT system damaging the NFC system due to too much energy being delivered. These investigations were conducted using time-efficient broadband circuit-level simulations and measurement-verified broadband equivalent circuit coil models.**

***Index Terms*—Coils, near-field communication, wireless power transfer.**

I. Introduction

IN RECENT years, researchers and engineers have been aiming to provide mobile devices with an increasing number of wireless interfaces [1], [2]. These wireless interfaces include magnetically resonant coupled systems for wireless charging via wireless power transfer (WPT) and wireless communication via near-field communication (NFC) [3], [4]. WPT systems usually require a communication link [5] between the transmitter (TX) and receiver (RX) device, which could be provided by NFC. Due to the interference of these magnetically resonant coupled systems, it is crucial to conduct a communication and power transfer analysis to enable and optimize their simultaneous operation. Both systems have to be designed with each other in mind to achieve good WPT performance and communication quality. Thus, this work will show a first complete system-level analysis investigating interfering WPT and NFC systems. Here, a system-level analysis refers to an analysis using a verified system prototype equivalent circuit (EC) model to investigate the systems' functionality and performance. The WPT system operates at the 6.78 MHz industrial, scientific, and medical (ISM) band. This frequency was used by the Alliance for Wireless Power (A4WP) and Powermat, which have merged to the AirFuel Alliance. The NFC system operates at 13.56 MHz. The work discusses a system using miniaturized coils (NFC class 6 [6]), suitable for small devices such as wearables and wristbands [7], [8].

The discussed related work on interfering magnetically resonant coupled systems is summarized in Tab. I. The table divides each work into its used WPT system and communication system, detailing the type of coupling, frequency, and coil form factor. Further, it details how the interference between the systems is analyzed and what solutions to mitigate the interference were introduced.

A group investigated magnetic resonant coupling-based power (12 MHz) and data ($90-135$ MHz) transfer [9], which are both operated outside of ISM frequency bands. A multiple-band configuration was proposed to separate power and data transfer frequencies, creating channels at different frequencies with multiple resonant circuits. The coil setup was measured to verify the resonance frequency of the resonant circuits via scattering parameters. However, neither the communication quality nor WPT performance were investigated. Another group conducted research regarding WPT (110 kHz) and NFC (13.56 MHz) interference [10]. The investigation is carried out using inductively coupled coils without resonant tuning. The interference is reduced via the coil winding layout, which is verified by scattering parameter measurements. However, the positive effects of inductive decoupling on the communication quality or WPT performance were not investigated. Further research was conducted regarding the inductive decoupling of coils [11]. Here, WPT (6.78 MHz) and NFC (13.56 MHz) interference was investigated. The WPT TX was tuned to a

Manuscript received 30 December 2023; revised 7 March 2024, 2 May 2024, and 5 July 2024; accepted 15 July 2024. Date of publication 29 July 2024; date of current version 30 August 2024. This work was supported by the "University SAL Labs" initiative of Silicon Austria Labs (SAL) and its Austrian Partner Universities for Applied Fundamental Research for Electronic-Based Systems. *(Corresponding author: Richard Fischbacher.)*

Richard Fischbacher and Jose Romero Lopera are with the Institute of Microwave and Photonic Engineering, Graz University of Technology, 8010 Graz, Austria, and also with Silicon Austria Labs, 8010 Graz, Austria (e-mail: richard.fischbacher@tugraz.at).

David Pommerenke is with the Institute of Electronics, Graz University of Technology, 8010 Graz, Austria, and also with Silicon Austria Labs, 8010 Graz, Austria (e-mail: richard.fischbacher@tugraz.at).

Ralph Prestros and Bernhard Auinger are with Silicon Austria Labs, 8010 Graz, Austria.

Wolfgang Bösch and Jasmin Grosinger are with the Institute of Microwave and Photonic Engineering, Graz University of Technology, 8010 Graz, Austria.

Digital Object Identifier 10.1109/JRFID.2024.3434642

TABLE I
RELATED WORK ON INTERFERING MAGNETICALLY RESONANT COUPLED SYSTEMS

Reference	WPT system Type	WPT system Antenna	Communication system Type	Communication system Antenna	Analysis of WPT and communication interference	Solution to mitigate interference
[9]	MRC[1] 12 MHz	Circular 36 mm radius	MRC[1] 90-135 MHz	Circular 36 mm radius	S-parameter analysis showing separate frequency bands	Frequency separation of WPT and NFC
[10]	Inductive 110 kHz	Square 50 mm	NFC (inductive) 13.56 MHz	Square 50 mm	S-parameter analysis showing reduced cross-coupling	Inductive decoupling via coil design
[11]	Inductive 6.78 MHz	Varying shapes	NFC (inductive) 13.56 MHz	Rectangular 117 x 62 mm	WPT efficiency analysis based on WPT and NFC coil displacement	Inductive decoupling via positioning
[14]–[16]	MRC[1] 106 kHz	Circular [17] 25 mm radius	NFC (MRC[1]) 13.56 MHz	Circular 17.5 mm radius	Communication analysis	Inductive decoupling
[18]	MRC[1] 6.78 MHz	Circular 5 mm radius	NFC (MRC[1]) 13.56 MHz	Circular 5 mm radius	Communication analysis	Inductive decoupling and system level adjustments
This work	MRC[1] 6.78 MHz	Circular 5 mm radius	NFC (MRC[1]) 13.56 MHz	Circular 5 mm radius	Communication and power transfer analysis	Inductive decoupling and system level adjustments

[1]Magnetic resonant coupling.

resonance frequency of 6.78 MHz, while the WPT RX was not tuned and was connected to a load resistance. A short-circuited NFC coil was used as a pick-up coil located between the TX and RX coil. The coupling between the WPT TX/RX and the pick-up coil was reduced via positioning, verified by measurement of the mutual inductance. However, the quality of communication was not investigated. Additionally, the WPT efficiency is given as a function of the pick-up coil position but was not investigated in relation to an NFC system prototype. Further, many researchers have investigated stand-alone magnetic resonant coupling-based WPT systems (7.65 − 13.56 MHz), with the intent to optimize the WPT performance [12], [13].

Our previous work focused on WPT and NFC interference analyses in circuit-level simulations [14], [15], [16]. A narrowband investigation regarding WPT interference on the NFC communication quality was conducted [16]. Behavioral and physical coil EC models [19] were introduced to allow broadband system level investigations [15]. Additionally, a WPT and NFC system prototype was verified via measurements and a preliminary broadband NFC communication analysis was conducted [14] using the low-frequency Qi WPT standard [5].

This work investigates, for the first time, interference issues regarding the NFC communication quality and the WPT performance of interfering WPT (ISM band: 6.78 MHz) and NFC (13.56 MHz) systems. The communication analysis is conducted by investigating the communication quality of the NFC tag-to-reader communication signal. In contrast to previous work, the communication signal is investigated in the digital baseband while being interfered with by WPT. The WPT performance is analyzed via maximum power transferred and the WPT efficiency η. Instead of stand-alone WPT analyses from previous work [12], [13], [20], the passive loading effects of NFC on the WPT system are investigated on a system level. Contrary to previous work, an NFC system prototype is used instead of a single pick-up coil [11]. It has also been investigated whether WPT can deliver too much energy to NFC tags, risking their destruction. Contrary to previous work, the effects of inductive decoupling [10], [11] are investigated on a system level, which aims

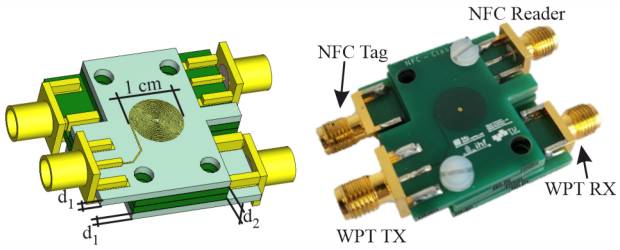

Fig. 1. Miniaturized WPT and NFC coils: The left-hand figure shows a schematic view of the coil stack. The right-hand figure shows the prototype.

to improve communication quality and WPT performance. A novel system level adjustment, discussed in the previous conference paper [18], regarding the communication signal demodulation, is introduced to improve the communication quality further. The investigations are conducted via broadband circuit-level simulations due to their time and computation efficiency compared to finite element (FEM) simulations [21]. A broadband approach is needed when system operating frequencies differ. Thus, broadband instead of narrowband EC models [12], [13], [20] are used, which were verified in our previous work [14], [15].

This work is the extended version of the authors' previous work [18]. The conference paper is expanded significantly by a more thorough communication analysis using larger data sets, a more realistic inductive decoupling approach, more inductive decoupling states, and a power transfer analysis.

The structure of this article is as follows. Section II details the generation and verification of the necessary coil EC models, Section III shows the NFC communication quality analysis, and Section IV shows the power transfer analysis.

II. INTERFERING MAGNETICALLY RESONANT COUPLED SYSTEMS

This section discusses the broadband EC model of the WPT and NFC system used in this work to conduct a communication and power transfer analysis via circuit-level simulation. The EC model consists of the coil and tuning circuit EC models. The coil EC model is generated via the measured impedance

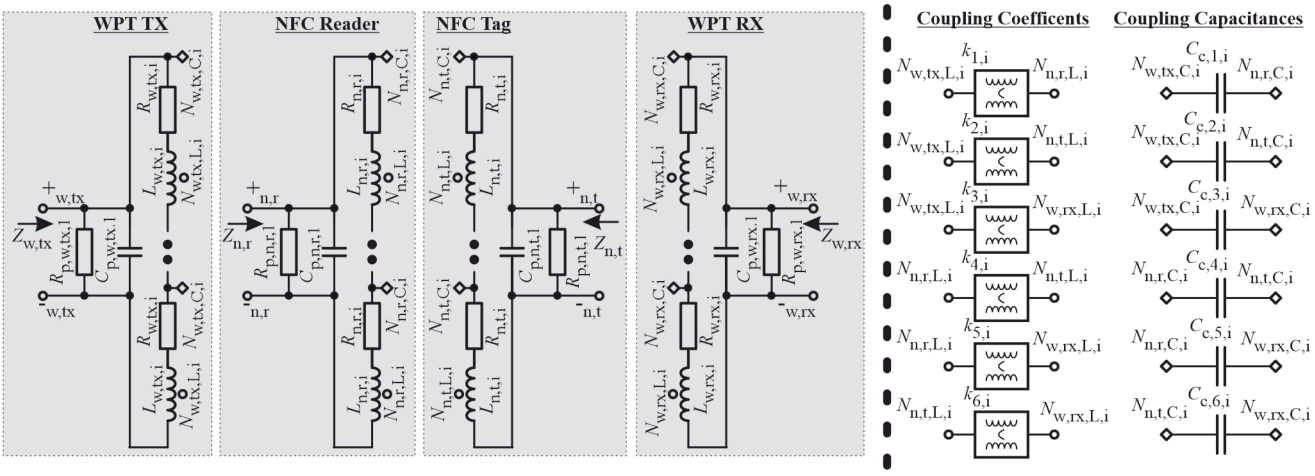

Fig. 2. Coupled coil EC model: The left-hand figure shows the coil EC models, while the right-hand figure shows the coupling interactions. The node names N highlight which coil and coupling interaction are connected. The tuning circuit connections are denoted with the + and − nodes (see Fig. 4). All coils are identical, and their component values are given with $L = 506$ nH, $R = 0.46\ \Omega$, $R_\mathrm{p} = 37.5\ \mathrm{k}\Omega$, and $C_\mathrm{p} = 1.7$ pF. The coupling coefficients $k_{1..6,i}$ and coupling capacitances $C_{\mathrm{c},1..6}$ are given in Tab. II. The following conditions need to be applied to the coils and the coupling capacitances: $L_i = L/10$, $R_i = R/10$, and $C_{\mathrm{c},1..6,i} = C_{\mathrm{c},1..6}/10$ for $i = 1..10$.

TABLE II
EC MODEL COUPLING VALUES (SEE FIG. 2) MODELING THE PROTOTYPE SHOWN IN FIG. 1

$u =$	1	2	3	4	5	6
$k_{u,i}$	0.371	0.094	0.054	0.19	0.092	0.373
$C_{\mathrm{c},u}$ (pF)	2.08	2.05	0.60	1.72	2.04	2.17

parameters Z of the WPT and NFC prototype coils. The prototype of the coils is shown in Fig. 1, where a TX (WPT TX and NFC reader) and RX (WPT RX and NFC tag) coil setup is shown. The four identical coils comply with the NFC class 6 form factor [6] and were manufactured on printed circuit boards (PCB, material: NP − 155F [22]) with 1 cm diameter, 11 windings, 0.2 mm width, and 35 μm thickness. The coil distances are given with $d_1 = 1.5$ mm and $d_2 = 3$ mm. The tuning circuits were designed following the low-frequency Qi WPT standard [5] and NFC system design guidelines [23].

A. Broadband Coil EC Models

This prototype is measured to generate the broadband coil EC model given in Fig. 2. The methodology is discussed in our previous work [15], strictly using directly measured values.

A simple EC model is generated consisting of the coil inductance L, DC resistance R, parallel resistance R_p, and parallel capacitance C_p (see Fig. 2). R_p models the real part at the coil resonance frequency (usually referred to as losses in the medium), while C_p models the parasitic coil capacitance to account for the self-resonant frequency of the coil [24]. The coupling coefficient $k_{1..6,i}$ and coupling capacitance $C_{\mathrm{c},1..6}$ between all coils are determined [15] (see Tab. II). Due to the voltage drop across the coil, the EC model of the coupled coils needs to be adjusted. The inductance and DC resistance are divided into ten parts [15], which enables the spreading of the coupling capacitance across the coil (see Fig. 2, $L_i = L/10$, $R_i = R/10$, and $C_{\mathrm{c},1..6,i} = C_{\mathrm{c},1..6}/10$).

Further, FEM simulations of the coil stack are conducted via CST [25] for verification. The coils were imported into CST via DXF files to match the prototype geometry. In CST, the standard material template for PCBs was used (FR-4 adjusted to NP − 155F [22]), and the CST metal copper (annealed) (metal type: normal) was used for the PCB traces. The SMA-connectors were modeled to match the prototype geometry.

To compare the measurement (M), FEM simulation, and EC model, the prototype was connected to a vector network analyzer (VNA, R&S ZVL) via baluns (WBC1-1TLC, Coilcraft) and a coaxial cable fitted with ferrite beads to drive the coils in a balanced manner and suppress sheath currents. Port 1 is connected to the WPT TX coil, port 2 is connected to the NFC reader coil, while the WPT RX and NFC tag coils are terminated with a 50 Ω resistance.

The comparison is shown in Fig. 3 via the magnitude of the impedance (Z) parameters (Z_{11}, Z_{12}, and Z_{22}). One can see excellent agreement between measurement and EC model from 0.1 to 500 MHz with minor issues at resonance peaks and troughs between 100 MHz and 200 MHz. The resonance frequencies show less than 5 % disagreements between measurement and EC model. Better agreement can be achieved by conducting parametric sweeps of the lumped components. The FEM simulation shows good qualitative agreement with measurement and EC model up to 300 MHz. It agrees well quantitatively at lower frequencies, but shifts in the magnitude and resonance frequencies can be seen starting at 130 MHz. In future work, ferrites will be added to the prototype, which cannot be modeled properly in simulation. Such ferrites introduce problems, as it is not very well understood how to determine their material parameters required for accurate FEM simulations, above low MHz frequencies [26]. Thus, qualitative agreements with FEM simulations are deemed satisfactory.

B. Tuning Circuits

The tuning circuits are given in Fig. 4 and were designed following the low-frequency Qi WPT standard [5] and NFC

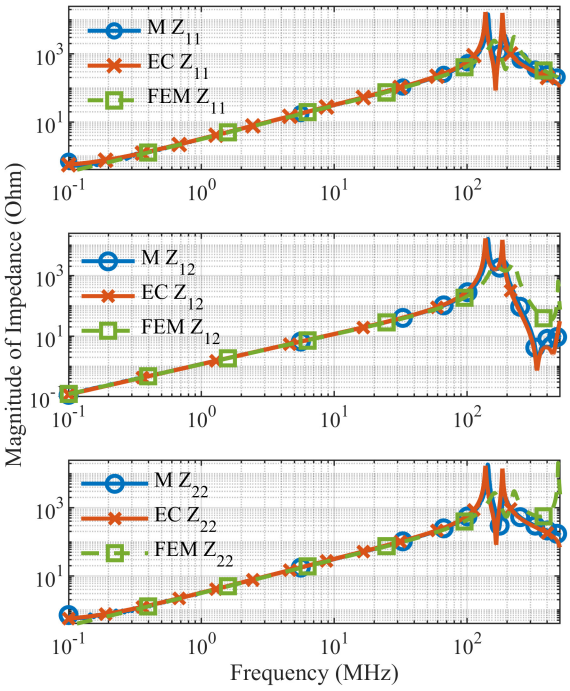

Fig. 3. Magnitude of impedance parameters of coil stack: Impedance parameters validate the EC model by comparing it to measurement (M) and FEM simulation results. Port 1 is connected to the WPT TX coil ($Z_{\mathrm{w,tx}}$, Fig. 2), port 2 is connected to the NFC reader coil ($Z_{\mathrm{n,r}}$, Fig. 2), and the WPT RX and NFC tag coil are terminated with a 50 Ω resistance.

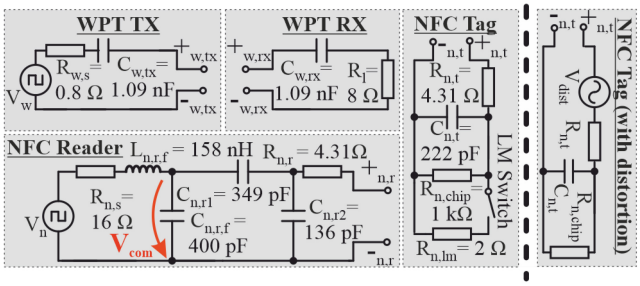

Fig. 4. WPT and NFC tuning circuits: The nodal connections to the coils shown in Fig. 2 are indicated with + and −. The lumped elements of the NFC reader circuit achieve a parallel resonance of the NFC reader at 13.56 MHz with 70 Ω for $k_{1,\mathrm{i}}$ given in Tab. II. The figure on the right shows a simplified tag tuning circuit, which includes a distortion source and no load modulation capabilities.

system design guidelines [23]. Their purpose is to enable magnetic resonant coupling at the desired frequencies.

The NFC reader is supplied with a square wave source ($V_{\mathrm{n,peak}} = 1.65$ V, 13.56 MHz [27]) with the inner resistance $R_{\mathrm{n,s}}$. $L_{\mathrm{n,r,f}}$ and $C_{\mathrm{n,r,f}}$ form a second-order low-pass filter to attenuate higher order harmonics of V_{n}. $C_{\mathrm{n,r1}}$ and $C_{\mathrm{n,r2}}$ are used to set the NFC reader resonance frequency to 13.56 MHz and its impedance to 70 Ω while being coupled to the WPT TX coil. The quality factor of the NFC reader and tag coil is adjusted with $R_{\mathrm{n,r/t}}$. $C_{\mathrm{n,t}}$ models a tuning capacitance combined with the NFC tag chip capacitance to achieve a tag resonance frequency of 15 MHz. The NFC tag resonance frequency is ideally higher (i.e., around 14.5 MHz to 15 MHz)

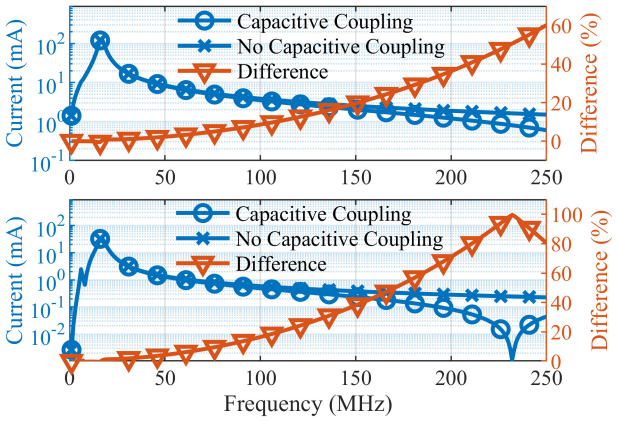

Fig. 5. Coil currents caused by distortion source: The tag coil (top) and reader coil (bottom) currents are shown for a distortion source (V_{dist}, see Fig. 4) for $V_{\mathrm{dist}} = 1$ V from 1 to 250 MHz. The currents are shown for the coil EC models (see Fig. 2) with and without capacitance coupling. Further, the difference of the two results is given in percent.

than the reader operating frequency (i.e., 13.56 MHz) to counteract card loading effects [28]. The chip real part is modeled with $R_{\mathrm{n,chip}}$ [28]. The load modulation (LM) switch shorts $R_{\mathrm{n,chip}}$ via the low-ohmic $R_{\mathrm{n,lm}}$ to achieve load modulation for tag-to-reader communication.

The WPT TX and RX are tuned to a series resonance at 6.78 MHz via $C_{\mathrm{w,tx/rx}}$. The WPT TX is supplied with a square wave source ($V_{\mathrm{w,peak}} = 3$ V [29], 6.78 MHz) with the inner resistance $R_{\mathrm{w,s}}$. The WPT RX tuning circuit is terminated with a battery equivalent resistance R_{l} [5]. The operating frequency of 6.78 MHz was chosen to allow small and thin one layer coils on PCBs to reach a reasonable coil quality factor for WPT. This specific coil achieves a quality factor of 46.

C. Capacitive Coupling

The following investigation is conducted to determine in which frequency range capacitive coupling has a relevant influence on the system behavior. Figure 4 shows a simplified NFC tag circuitry on the right. It uses the same values as in the above-described tag circuitry without load modulation switch and resistance but includes a distortion source (V_{dist}). The simplified circuitry replaces the standard NFC tag circuitry for this investigation. The distortion source supplies a sine with 1 V magnitude and variable frequency, simulating a picked-up electromagnetic interference by the tag coil.

In Fig. 5, the resulting current through the tag and reader coil inductance are highlighted versus frequency, ranging from 1 to 250 MHz. The current is shown for the EC model with and without capacitive coupling. This frequency range was chosen to cover the self-resonance frequency of the coils at 171 MHz. Additionally, the difference between the currents for capacitive and no capacitive coupling is given in percent. As expected, capacitive coupling at lower frequencies (WPT/NFC operation frequencies) does not affect the system but gains importance with increasing frequencies as errors of up to 110 % are shown above 200 MHz. Thus, capacitive coupling is important if high-order harmonics are discussed.

TABLE III
TUNING CAPACITANCE VALUES FOR SPECIFIC INDUCTIVE DECOUPLING (IDEC)

IDEC (%)	0	5	10	15	20	25	30	35	40	45	50	55	60	65	70	75	80	85	90
$C_{\mathrm{n,r1}}$ (pF)	549	487	441	406	374	351	331	313	299	288	277	268	261	254	249	246	242	240	238
$C_{\mathrm{n,r2}}$ (pF)	162	156	150	145	142	139	134	133	129	127	125	122	121	119	118	118	117	116	116

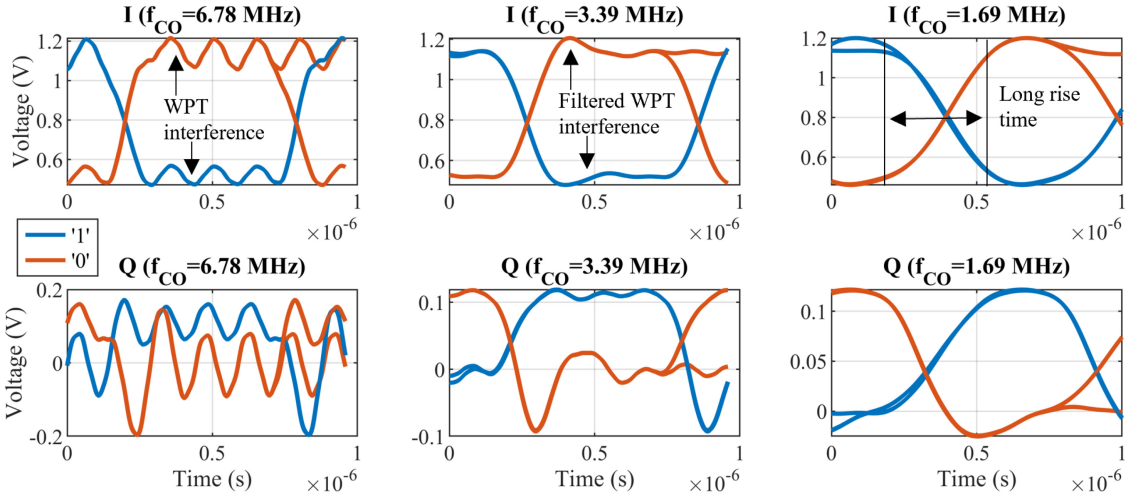

Fig. 6. Eye diagram of V_{com}: The eye diagram of the I/Q components of V_{com} are shown versus time for different I/Q demodulation low-pass filter cut-off frequencies $f_{\mathrm{CO}} = 1.69, 3.39$, and 6.78MHz. Each logical state consists of 29 overlaps, each recorded at a different time during the communication sample. The start of logic state '1' and end of logical state '0' show two different trajectories each, due to Manchester encoding.

III. COMMUNICATION ANALYSIS

The communication analysis investigates the NFC tag-to-reader communication quality while the WPT system interferes with the NFC system. The coupling coefficients between the coils can vary drastically depending on each implementation and specific use case. The main determining factors of the coupling coefficients are the coil distance, co-planar alignment, and coaxial alignment [3]. For a more general analysis of the NFC communication quality, we adjust the EC model coupling values shown in Tab. II to model a stronger coupling between the individual coils. This adjustment of the EC model is feasible as measurements have validated the EC model. In addition, its synthesis has been tested using another prototype with different-sized coils [15].

In particular, the TX and RX in wireless charging and NFC applications usually directly contact their casing. We can assume that higher coupling coefficients than given in the coil stack prototype can be achieved (see Tab. II), as the prototype shown in Fig. 1 is limited to small WPT coupling coefficients by the 1.5 mm thick PCBs. These changes result in a more realistic analysis. The adjusted coupling coefficients are given in Tab. IV, which is a reasonable coupling coefficient range according to our previous work [14], [15], where we used an NFC coupling coefficient of $k = 0.45$.

The coupling coefficients between the WPT coils ($k_{3,i}$) and NFC coils ($k_{4,i}$) are kept constant. The system cross-coupling coefficients ($k_{1,i}$, $k_{2,i}$, $k_{5,i}$, and $k_{6,i}$) are varied by multiplication with the factor y_{cpl} ($y_{\mathrm{cpl}} = 0.1$ equates to inductive decoupling of 90 %). This factor models inductive decoupling between WPT and NFC as proposed in [10], [11]. The NFC reader should operate at 13.56 MHz with 70 Ω resistance [23]. This tuning state is achieved while being coupled to the WPT TX coil, as both are part of the same TX device. The specific values per inductive decoupling are given in Tab. III. Such an inductive decoupling, achieved by novel coil design or horizontal coils misalignment causes lower coupling coefficients. Thus, it is equivalent to a larger coil distance and enables engineers to design small and thin devices with reduced WPT and NFC interference.

TABLE IV
ADJUSTED EC MODEL COUPLING VALUES (SEE FIG. 2) FOR COMMUNICATION QUALITY ANALYSIS

$u =$	1	2	3	4	5	6
$k_{u,i}$	0.5	0.35	0.3	0.4	0.35	0.5
$C_{\mathrm{c},u}$ (pF)	2.08	2.05	0.60	1.72	2.04	2.17

A. I/Q Demodulation of the Communication Signal

The NFC tag-to-reader communication is simulated by changing the load modulation switch state with twice 847.5 kHz with Manchester encoding for type A ISO/IEC 14443 communication [6]. The setup is not limited to type A communication and can be used for binary phase shift keying. This is achieved by changing the load modulation switching sequence to conduct communication at higher data rates (type B [6]). The communication signal is determined with the voltage V_{com} at the NFC reader (see Fig. 4) [16] and it is I/Q demodulated [30]. The required low-pass filter (usually part of the NFC reader) is generated in a post-processing task with a fourth-order Butterworth filter.

Figure 6 shows the logical states of V_{com} for I and Q versus time with an eye diagram. The logical state '1' is defined by

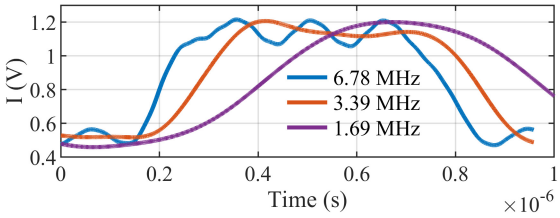

Fig. 7. Eye diagram of V_{com}: The eye diagram of logical state '0' of the I component of V_{com} is shown versus time for different I/Q demodulation low-pass filter cut-off frequencies $f_{CO} = 1.69, 3.39$, and 6.78MHz. One sample of the 29 overlaps from Fig. 6 is shown.

a closed load modulation switch and the logical state '0' is defined with an open load modulation switch. The inductive decoupling is set to 90 % and the a Butterworth filter cut-off frequency is set to $f_{CO} = 1.69, 3.39$, and 6.78 MHz. This cut-off frequency is usually used to filter convolution products of the NFC carrier created by the I/Q demodulation. It can usually be set high enough to barely interfere with the communication signal. In this use-case, the cut-off frequency can additionally be used to filter the 6.78 MHz WPT signal. Thus, a trade-off between the filtering of the WPT signal while preserving the 847.5 kHz communication signal square wave has to be chosen. This combination of NFC carrier frequency 13.56 MHz, communication signal modulation frequency 847.5 kHz, and filter cut-off frequency 6.78 MHz was used in previous work with a low-frequency Qi-WPT system operating at 106 kHz [14]. Due to the low WPT frequency, the Butterworth filter was only used to separate the NFC carrier from the communication signal after I/Q demodulation.

In this work, a higher frequency WPT system operating at 6.78 MHz is used, which leads to the WPT signal significantly interfering with the I and Q components (ripple superposed with the square wave) for $f_{CO} = 6.78$ MHz. Strong inductive decoupling still allows for a clear distinction of the logical states via the I component but not the Q component. The filter cut-off frequency can be used as a design parameter. Decreasing the cut-off frequency to $f_{CO} = 3.39$ MHz, shows good filtering of the WPT influence, leading to distinct logical states for the I and Q component while preserving the square wave shape of the communication signal. Reducing the cut-off frequency further to $f_{CO} = 1.69$ MHz shows even better filtering of the WPT influence. Although it is too close to the base frequency of the 847.5 kHz communication square wave, which causes severe degradation of the square wave shape, which is highlighted in Fig. 7. This figure shows the logical state '0' of I for $f_{CO} = 1.69, 3.39$, and 6.78 MHz versus time. One can see the trade-off between suppressing the WPT signal (superposed ripple for 6.78 MHz) and preserving the square wave shape (long rise time and sine shape for 1.69 MHz). Thus, it can be concluded that the Butterworth low-pass filter cut-off frequency could be an essential tool to improve the communication quality of NFC systems being interfered with by WPT systems.

B. Signal Constellation Diagram Analysis

Figure 8 shows the eye diagram and signal constellation diagram of I and Q for 70 % inductive decoupling and

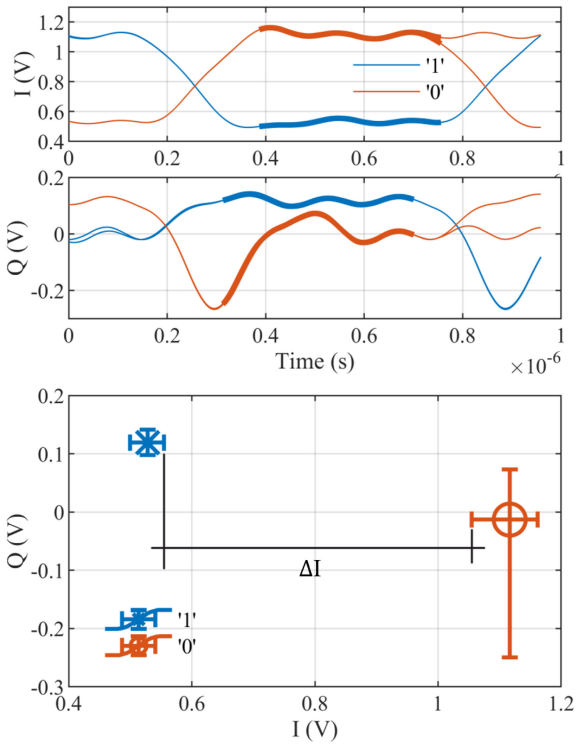

Fig. 8. Signal constellation diagram: The top two figures show the I/Q components of V_{com} for $f_{CO} = 3.39$ MHz for 70 % inductive decoupling. The thick lines indicate which values are recorded and converted to the signal constellation diagram in the third figure. Error bars indicate the minimum and maximum values for I and Q. The mean values are indicated by the cross-section of the error bars. ΔI indicates the difference between the minimum I value of the logical state '0' and the maximum I value of the logical state '1.'

$f_{CO} = 3.39$ MHz versus time [31]. In the signal constellation diagram, Q is plotted versus I. The error bars indicate the minimum and maximum value for each logical state. The mean values of I and Q for a logical state are indicated by the intersection of the error bars. This particular state of inductive decoupling and f_{CO} shows a clear distinction of the logical states via I, as the distance between the minimum value for logical state '0' and the maximum value for logical state '1' show a significant difference ΔI (see Fig. 8). The Q error bars show no overlap but have a smaller difference. Thus, the logical states are distinct for both the I and Q components, indicating that an NFC reader should be able to detect the NFC tag communication signal.

The difference between the I and Q error bars (ΔI and ΔQ) is shown to compare larger data sets. These are plotted versus inductive decoupling for $f_{CO} = 3.39$ MHz and 6.78 MHz in Fig. 9. Here, a positive value indicates a certain distance between error bars. In contrast, a negative value indicates an overlap, i.e., non-distinct logical states (likely a communication failure). The I component is the focus of this investigation as this type of NFC communication is mainly an amplitude modulation, i.e., large I component and small Q component. Larger system cross-coupling (i.e., decreased inductive decoupling) causes the difference between the error bars (ΔI and ΔQ) to turn negative for both I and Q in Fig. 9. As shown before in Fig. 6, $f_{CO} = 3.39$ MHz shows more

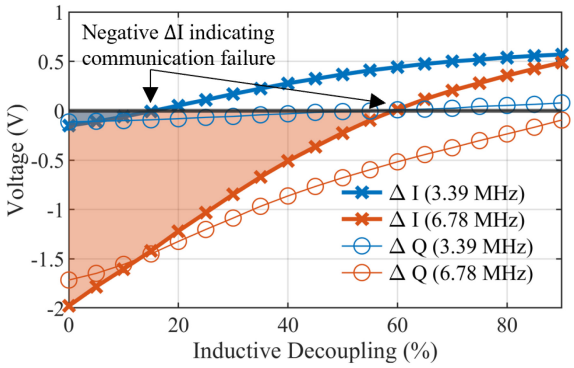

Fig. 9. Difference between logical states for $f_{CO} = 3.39$ MHz and 6.78 MHz: ΔI and ΔQ are shown for the difference between the logical states '0' and '1' for I and Q for all inductive decoupling values.

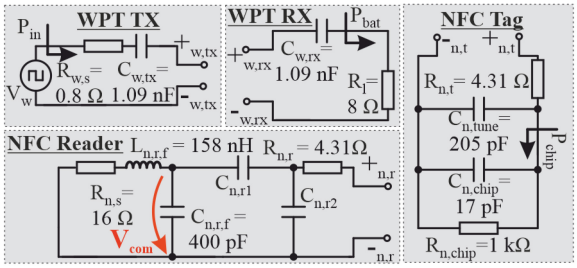

Fig. 10. WPT and NFC tuning circuits: The nodal connections to the coils shown in Fig. 2 are indicated with + and −. The NFC reader source and NFC tag load modulation switch are removed. The input power P_{in}, battery power P_{bat}, and NFC tag chip power P_{chip} are indicated.

distinct logical states than $f_{CO} = 6.78$ MHz (i.e., higher likelyhood of the NFC reader successfully detecting the NFC tag signal). It is shown that lower f_{CO} provides a logical state distinction up to much weaker inductive decoupling. A negative difference of I is shown for smaller than 15 % decoupling with $f_{CO} = 3.39$ MHz, but $f_{CO} = 6.78$ MHz requires an inductive decoupling of more than 60 %. Thus, this communication investigation indicates that inductive decoupling techniques [10], [11] are effective. The WPT interference is decreased, which increases the likelihood of successful NFC tag-to-reader communication due to more separate logical '0' and '1' states. Additionally, novel adjustments, such as optimizing the post-processing via the I/Q demodulation cut-off frequency, can additionally improve the NFC tag-to-reader communication quality.

IV. WPT Analysis

This section discusses an investigation of the WPT system performance concerning passive loading effects caused by the NFC system [4], [6]. Thus, the NFC source (V_n) is turned off, and no load modulation is performed. The simplified NFC circuitries are shown in Fig. 10. The passive loading effects include the NFC system drawing power, detuning the WPT TX, and changing the impedance seen from the WPT TX.

The tag chip impedance can vary greatly [28], significantly influencing NFC's passive loading effects. The tag chip resistance $R_{n,chip}$ is varied from 1 Ω to 10 kΩ, which includes possible tag impedance changes caused by the reduced tag chip impedance during communication, the overvoltage protection of a tag chip via its limiter [28], and the usual high-ohmic state while the tag is listening to the reader. The changes of the tag chip capacitance are ignored as they are small compared to $C_{n,t}$.

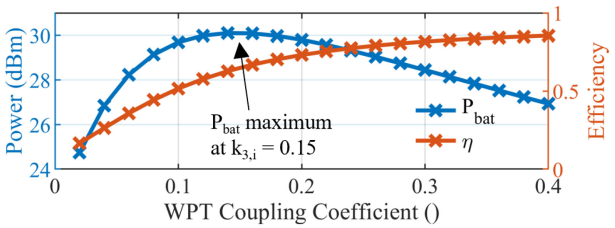

Fig. 11. WPT analysis: The battery power P_{bat} and the WPT efficiency η are plotted versus the WPT coupling coefficient $k_{3,i}$ while all other coupling coefficients are kept constant as shown in Tab VI.

The power supplied by the WPT source (P_{in}), the received power by the WPT battery equivalent resistance (P_{bat}), and the received power by the NFC tag chip (P_{chip}) are determined. This requires us to divide $C_{n,t}$ into a tuning capacitance $C_{n,tune}$ and into a tag chip capacitance $C_{n,chip}$ ($C_{n,t} = C_{n,tune} + C_{n,chip}$). The WPT system was examined to find the coupling arrangement for maximum power transfer from P_{in} to P_{bat}. The bifurcation phenomena of $|S_{21}|$ [12], [32] do not align with the power transfer maximum due to different WPT source ($R_{w,s}$) and battery (R_l) impedance. Thus, the received power P_{bat} is shown directly instead of an S-parameter magnitude plot. Further, the system's efficiency is defined via $\eta = P_{bat}/P_{in}$.

Again, as done before in Section III, we adjust the EC model coupling values shown in Tab. II to model coupling coefficients suitable for the power transfer analysis performed in this section. When the WPT system is operated on its own, a coupling coefficient for optimal power transfer of $k_{3,i} = 0.16$ is determined. The previously adjusted coupling coefficients given in Tab. IV are too large, as adding the NFC system further loads the WPT system, reducing the optimal coupling coefficient to 0.1. This is caused by the fact that the coils operate in the near-field of each other, and thus, the NFC system is seen as a reflected impedance from the WPT TX point of view [33], [34]. The WPT system was designed to operate with P_{bat} being maximised. Halving each coupling coefficient of Tab. IV leads to a good operating window at $k_{3,i} = 0.15$. The resulting coupling coefficients are given in Tab. VI. Thus, the same tuning elements for the NFC reader tuning circuitry from Tab. III for 50 % inductive decoupling can be used.

Figure 11 shows P_{bat} and η versus a swept WPT coupling coefficient $k_{3,i}$ while the other coupling coefficients are kept constant. A maximum of P_{bat} can be seen at $k_{3,i} = 0.15$ and the efficiency increases as $k_{3,i}$ increases. The coupling coefficients are chosen to be different from Section III, because the previous section aimed to determine the issues in regards to WPT interference, which are worse if particularly strong coupling is used. Contrary to that, here we investigate the WPT performance and thus, want to investigate the WPT system at the coupling point of maximum power transfer. Thus, all coupling coefficients must be adjusted to achieve a realistic coupling state between all coils.

TABLE V
TUNING CAPACITANCE VALUES FOR SPECIFIC INDUCTIVE DECOUPLING (IDEC)

IDEC (%)	0	5	10	15	20	25	30	35	40	45	50	55	60	65	70	75	80	85	90
$C_{\mathrm{n,r1}}$ (pF)	277	273	269	264	261	258	254	252	249	247	246	244	242	241	240	239	238	237	236
$C_{\mathrm{n,r2}}$ (pF)	125	123	122	122	121	120	119	119	118	118	118	117	117	116	116	116	116	116	116

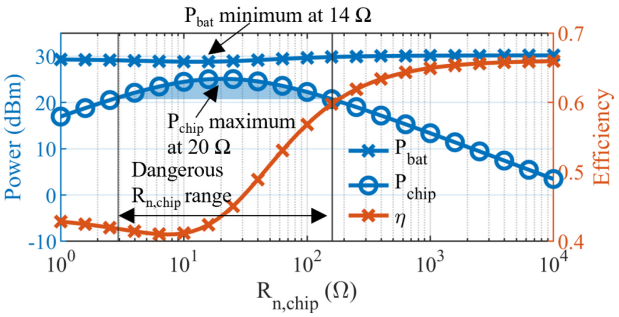

Fig. 12. Chip impedance sweep: The received battery power P_{bat}, tag chip power P_{chip}, and the WPT efficiency η are plotted versus the tag chip resistance $R_{\mathrm{n,chip}}$.

TABLE VI
ADJUSTED EC MODEL COUPLING VALUES (SEE FIG. 2) FOR WIRELESS POWER TRANSFER ANALYSIS

$u =$	1	2	3	4	5	6
$k_{u,i}$	0.25	0.175	0.15	0.2	0.175	0.25
$C_{\mathrm{c},u}$ (pF)	2.08	2.05	0.60	1.72	2.04	2.17

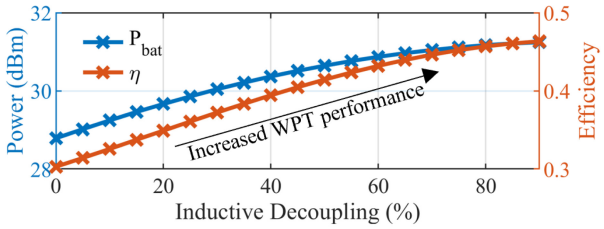

Fig. 13. WPT analysis with inductive decoupling: The received battery power P_{bat} and the WPT efficiency η are plotted versus inductive decoupling for the P_{bat} minimum shown in Fig. 12 ($R_{\mathrm{n,chip}} = 14\ \Omega$).

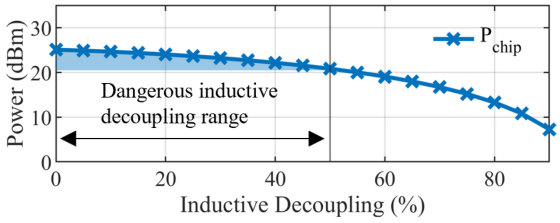

Fig. 14. Received tag chip power with inductive decoupling: The received tag chip power P_{chip} is plotted versus inductive decoupling for the P_{chip} maximum shown in Fig. 12 ($R_{\mathrm{n,chip}} = 20\ \Omega$).

Figure 12 shows P_{bat}, P_{chip}, and the WPT efficiency η for a changing tag impedance. The tag can receive dangerous power levels P_{chip} from the WPT source in the 3 Ω to 150 Ω range, when comparing the received P_{chip} to power dissipation limits of tag chip datasheets (20.7 dBm = 120 mW [35] or 23.8 dBm = 240 mW [36]). The P_{chip} maximum of 25.1 dBm = 324 mW is reached at $R_{\mathrm{chip}} = 20\ \Omega$. Further, $R_{\mathrm{n,chip}} = 14\ \Omega$ causes a P_{bat} minimum at 28.7 dBm = 0.75 W compared to the P_{bat} maximum at 30.1 dBm = 1.02 W. Additionally, WPT efficiency η is significantly affected by $R_{\mathrm{n,chip}}$ as it ranges from 0.42 to 0.67. These investigations highlight that passive loading caused by an NFC system can significantly degrade the WPT performance. It is especially important to note that these passive loading effects are dynamic, as the $R_{\mathrm{n,chip}}$ resistance is varied during normal operation due to NFC tag-to-reader communication and the tag chip overvoltage protection.

As suggested in prior literature [10], [11], inductive decoupling is applied to the system as discussed in Section III. Since the base coupling coefficients were changed from Tab. IV to Tab. VI, different inductive decoupling requires new tuning for the NFC reader. The new capacitance values are given in Tab. V. Figure 13 shows P_{bat} and η for $R_{\mathrm{n,chip}} = 14\ \Omega$ versus inductive decoupling from 0 to 90 % for $k_{1,i}$, $k_{2,i}$, $k_{5,i}$, and $k_{6,i}$. The clear benefits of WPT and NFC decoupling can be observed by an increased P_{bat} of up to 2.45 dBm. Further, inductive decoupling can have a significantly positive effect on the WPT performance by increasing the WPT efficiency η with increasing inductive decoupling. Inductive decoupling of WPT and NFC also has positive side effects for the NFC tag. Figure 14 shows the power P_{chip} versus inductive decoupling for $R_{\mathrm{n,chip}} = 20\ \Omega$. It shows how P_{chip} can be reduced below dangerous levels for tag chips as compared to Fig. 12. It can be concluded that the NFC system's passive loading severely impacts the WPT system. It is shown that the wide range of possible tag impedances has a large impact and that inductive decoupling can improve the maximum power transferred and the WPT efficiency η significantly. Additionally, it can prevent damage to the NFC tag.

V. CONCLUSION

This work provides a thorough communication and power transfer analysis of interfering magnetically resonant coupled WPT and NFC systems with miniaturized coils.

The communication analysis is conducted by investigating the NFC tag-to-reader communication quality in the digital baseband while being interfered with by WPT. The power transfer analysis is conducted by investigating the maximum power transferred and WPT efficiency η, while being affected by the passive loading effects of the NFC prototype system. The communication analysis showed that good communication quality, indicated by distinct logical states, required at least 60 % inductive decoupling. Further, novel system-level adjustments of the I/Q demodulation achieved distinct logical states, requiring only 15 % inductive decoupling.

The WPT analysis showed that the passive loading effects of NFC on the WPT performance reduces the maximum power transfer and WPT efficiency η. The performance degradation is dynamic, caused by the changing NFC tag chip impedance during active NFC communication or because of the over-voltage protection. It is shown that inductive decoupling can increase the WPT performance by increasing the maximum power transferred by up to 27 % and WPT efficiency η from 0.42 to 0.67. Inductive decoupling can prevent the WPT system from damaging the NFC system due to delivering too much energy. The analysis is conducted using time-efficient circuit-level simulations. The coils are modeled via broadband EC models and thoroughly verified via measurement and FEM simulation. The required tuning circuitry is based on NFC and WPT standards.

The quantitative results are specific to the selected parameters, but the presented methodologies can aid engineers and researchers with the iterative design process of magnetically resonant coupled systems. Inductive decoupling can benefit such interfering systems because a reduced coupling coefficient will always decrease interference and passive loading effects. The adjusted I/Q demodulation improves the NFC tag-to-reader communication quality by attenuating WPT interference of a higher frequency than the communication signal. Thus, it is most effective if the WPT frequency is larger than the communication signal frequency. It is to be noted that even systems using low-frequency WPT can cause high-frequency harmonics, which might be an issue in case of poor NFC reader and tag coil alignment, causing poor inductive coupling. Additionally, these novel optimization possibilities regarding WPT and NFC systems on a system level are investigated for the first time.

Ultimately the presented analysis aims to highlight problems and possible solutions to solve issues related to interfering magnetically resonant coupled systems. Future work has to focus on verifying the circuit-level solutions via additional measurements using state-of-the-art chargers and wearables. Additionally, further research is needed to determine the impedances and general behavior of NFC tags. Further, a self-jamming cancellation method [37] could potentially be used to dampen the WPT signal coupled into the NFC system.

REFERENCES

[1] M. Rajabi, N. Pan, S. Claessens, S. Pollin, and D. Schreurs, "Modulation techniques for simultaneous wireless information and power transfer with an integrated rectifier–receiver," *IEEE Trans. Microw. Theory Tech.*, vol. 66, no. 5, pp. 2373–2385, May 2018.

[2] J. Grosinger, W. Pachler, and W. Bösch, "Tag size matters: Miniaturized RFID tags to connect smart objects to the Internet," *IEEE: Microw. Mag.*, vol. 19, no. 6, pp. 101–111, Aug. 2018.

[3] J. Grosinger, "Robustly operating: Passive near-field communication systems in metal environments," *IEEE Microw. Mag.*, vol. 24, no. 4, pp. 30–39, Apr. 2023.

[4] *Information Technology—Telecommunications and Information Exchange Between Systems—Near Field Communication—Interface and Protocol*, ISO/IEC 18092:2013, 2013.

[5] *The Qi Wireless Power Transfer System Power Class 0 Specification, Version 1.2.3*, Wireless Power Consortium, Piscataway, NJ, USA, Feb. 2017.

[6] *Identification Cards—Contactless Integrated Circuit Cards—Proximity Cards*, ISO/IEC 14443-1:2016, 2018.

[7] "NXP Semiconductors." Wearables. 2023, Accessed: Sep. 1, 2023. [Online]. Available: https://bit.ly/407n8ii

[8] M. Wagih et al., "Microwave-enabled Wearables: Underpinning technologies, integration platforms, and next-generation roadmap," *IEEE Trans. Microw.*, vol. 3, no. 1, pp. 193–226, Jan. 2022.

[9] M. Dionigi and M. Mongiardo, "Multi band resonators for wireless power transfer and near field magnetic communications," in *Proc. IEEE MTT-S Int. Microw. Workshop Ser. Innovat. Wireless Power Transm., Technol., Syst., Appl.*, Kyoto, Japan, 2012, pp. 61–64.

[10] S. Hong et al., "Dual-directional near field communication tag antenna with effective magnetic field isolation from wireless power transfer system," in *Proc. IEEE Wireless Power Transfer Conf.*, Taipei, Taiwan, 2017, pp. 1–3.

[11] M. Kang, E. Noh, and K. Kim, "NFC transmitter coil placement to Minimize degradation of A4WP wireless power transfer efficiency," *Electron. Lett.*, vol. 53, pp. 616–618, Mar. 2017.

[12] A. P. Sample, D. A. Meyer, and J. R. Smith, "Analysis, experimental results, and range adaptation of magnetically coupled resonators for wireless power transfer," *IEEE Trans. Ind. Electron.*, vol. 58, no. 2, pp. 544–554, Feb. 2011.

[13] A. P. Sample, B. H. Waters, S. T. Wisdom, and J. R. Smith, "Enabling seamless wireless power delivery in dynamic environments," *Proc. IEEE*, vol. 101, no. 6, pp. 1343–1358, Jun. 2013.

[14] R. Fischbacher et al., "Communication quality analysis for WPT and NFC systems via broadband equivalent circuit models," *IEEE Antennas Wireless Propag. Lett.*, vol. 23, pp. 4–8, 2024.

[15] R. Fischbacher, D. Pommerenke, R. Prestros, J. R. Lopera, W. Bösch, and J. Grosinger, "Broadband EC models of coil antennas for inductively coupled systems," in *Proc. IEEE Wireless Power Week (WPW)*, Boredaux, France, 2022, pp. 465–469.

[16] R.Fischbacher et al., "EC model for WPT and NFC systems Interoperability analysis," in *Proc. IEEE Radio Wireless Symp. (RWS)*, San Diego, CA, USA, 2021, pp. 112–115.

[17] *WE-WPCC Wireless Power Transfer Transmitter Coil 760308101410*, Würth Elektronik, Waldenburg, Germany. Accessed: Sep. 1, 2023.

[18] R. Fischbacher, J. R. Lopera, D. Pommerenke, R. Prestros, W. Bösch, and J. Grosinger, "WPT and NFC Interoperability for Wearables with Miniaturized coils," in *Proc. IEEE RFID-TA*, Aveiro, Portugal, 2023, pp. 1–4.

[19] J. C. Pedro and S. A. Maas, "A comparative overview of microwave and wireless power-amplifier behavioral modeling approaches," *IEEE Trans. Microw. Theory Tech.*, vol. 53, no. 4, pp. 1150–1163, Apr. 2005.

[20] B. Deutschmann, L. Görtschacher, P. Priller, and J. Grosinger, "Efficient assessment of the impact of metallic obstacles on the wireless power transfer in loosely coupled links," in *Proc. 49th Eur. Microw. Conf.*, Paris, France, 2019, pp. 579–582.

[21] M. B. Steer, J. W. Bandler, and C. M. Snowden, "Computer-aided design of RF and microwave circuits and systems," *IEEE Trans. Microw. Theory Tech.*, vol. 50, no. 3, pp. 996–1005, Aug. 2002.

[22] "NP-155FTL, NP-155FR, NP-155FB," Data sheet, Technolam, Troisdorf, Germany, 2019.

[23] (NXP Semicond., Eindhoven, The Netherlands). *PN7120 Antenna Design and Matching Guide*. 2016. Accessed: Sep. 1, 2023. [Online]. Available: https://bit.ly/2CdlIgL

[24] T. Bauernfeind, W. Renhard, S. Schmethanner, M. Gebhard, and K. Preis, "Equivalent circuit parameter extraction for controlled detuned NFC antenna systems utilizing thin ferrite foils," in *Proc. 12th Int. Conf. Telecommun.*, Zagreb, Croatia, 2013, pp. 251–256.

[25] "CST studio suite." Dassault Systèmes. Accessed: Sep. 1, 2023. [Online]. Available: https://www.3ds.com/products/simulia/cst-studio-suite

[26] R. Fischbacher et al., "On the difficulties to determine the intrinsic material parameters for MnZn ferrites," in *Proc. Int. Symp. Exhibit. Electromagn. Compat.*, Kraków, Poland, 2023, pp. 1–6.

[27] "NFC controller with integrated firmware, supporting all NFC forum modes," Data sheet PN7120, NXP Semicond., Eindhoven, The Netherlands, 2018.

[28] J. Grosinger, B. Deutschmann, L. Zöscher, M. Gadringer, and F. Amtmann, "HF RFID tag chip impedance measurements," *IEEE Trans. Instrum. Meas.*, vol. 71, pp. 1–11, Nov. 2021.

[29] "700 mA dual H-Bridge motor driver with 3.0 V compatible logic I/O," Data sheet MPC17531A, NXP Semicond., Eindhoven, The Netherlands, 2016.

[30] J. Finol and M. Buchholz, "Design of an Inphase and quadrature phase and amplitude imbalance compensation in quadrature receivers," in *Proc. 5th IEEE Int. Caracas Conf. Devices, Circuits Syst.*, Punta Cana, Dominican, 2005, pp. 254–258.

[31] L. Görtschacher and J. Grosinger, "UHF RFID sensor system using tag signal patterns: Prototype system," *IEEE Antennas Wireless Propag. Lett.*, vol. 18, pp. 2209–2213, 2019.
[32] J. R. Lopera, R. Fischbacher, D. Pommerenke, R. Prestros, B. Auinger, and J. Grosinger, "Adaptive NFC WPT system implementing neural network-based impedance matching with bypass functionality," in *Proc. Int. Microw. Symp.*, San Dieago, CA, USA, 2023, pp. 879–882.
[33] C. Wang, G. Covic, and O. Stielau, "Power transfer capability and bifurcation phenomena of loosely coupled inductive power transfer systems," *IEEE Trans. Ind. Electron.*, vol. 51, no. 1, pp. 148–157, Feb. 2004.
[34] A. Laha, A. Kalathy, M. Pahlevani, and P. Jain, "A comprehensive review on wireless power transfer systems for charging portable electronics," *Eng*, vol. 4, no. 2, pp. 1023–1057, Feb. 2023.
[35] *Datasheet of NFC Tag MIFARE DESFire Light*, NXP Semicond., Eindhoven, The Netherlands. Accessed: Sep. 1, 2023.
[36] *Datasheet of NFC Tag MIFARE DESFire EV3*, NXP Semicond., Eindhoven, The Netherlands. Accessed: Sep. 1, 2023.
[37] A. S. Boaventurea and N. B. Carvalho, "Investigation on self-jamming suppression in passive RFID when using multisines to enhance wireless power transfer," in *Proc. IEEE Wireless Power Transf. Conf. (WPTC)*, Boulder, CO, USA, 2015, pp. 1–3.

Richard Fischbacher (Graduate Student Member, IEEE) received the Dipl.-Ing. (M.Sc.) degree (Hons.) in electrical engineering from the Graz University of Technology, Graz, Austria, where he currently pursuing the Ph.D. degree with the Institute of Microwave and Photonic. His master's thesis examined the capacitive coupling between a co-planar parallel-plate capacitor and an HF RFID coil antenna. The focus of this work, was to generate a model in a circuit-level environment, which was validated by finite element simulations. Since 2018, he has been a Project Assistant with the Institute of Microwave and Photonic Engineering, Graz University of Technology. His current research interests include RFID and WPT technologies. Here, he is specifically interested in the modeling of coil antennas in a circuit-level environment and the interoperability of NFC and WPT.

Jose Romero Lopera (Student Member, IEEE) received the Dipl.Ing. degree in industrial engineering from the Polytechnic University of Valencia, Spain, in 2012, and the Dipl.Ing. (M.Sc.) degree in electrical engineering from the Graz University of Technology, Graz, Austria, in 2017. In 2017, he enrolled in a Ph.D. position offered by the Institute of Microwave and Photonic Engineering, Graz University of Technology. In 2022, he is in the final stage of his Ph.D. During his ongoing Ph.D. Thesis, he worked with GaAs and GaN processes to design fully integrated MMIC RF power amplifiers, focusing on designing an MMIC Doherty RF Power Amplifier at Ka-band for space applications in GaN semiconductor technology. He had several internships at the British RF Consultancy VIPER RF, where he was involved in various industrial research projects dealing with RF MMIC Design. To date, he has authored five peer-reviewed publications and is also a member of the IEEE Microwave Theory and Techniques Society.

David Pommerenke (Fellow, IEEE) received the Diploma and Ph.D. degrees in electrical engineering from the Technical University Berlin, Berlin, Germany, in 1990 and 1996, respectively. He worked for five years in EMC with Hewlett Packard, Roseville, CA, USA, and joined the Faculty of the Electromagnetic Compatibility Laboratory, Missouri University of Science and Technology, Rolla, MO, USA. In 2020, he joined the Faculty of the EMC Laboratory, Graz University of Technology, Graz, Austria. His current research interests include system level ESD, electronics, numerical simulation, EMC, measurement methods, and instrumentation. He is an Associate Editor of the IEEE TRANSACTIONS ON ELECTROMAGNETIC COMPATIBILITY.

Ralph Prestros (Member, IEEE) received the M.Sc. degree (Hons.) in electrical engineering from the Technical University of Vienna, Austria, in 2003. He was with Infineon Technologies until 2008, where he was involved in contactless smart-card testing and represented Infineon and Austria in various international standardization bodies. In 2008, he joined the Application Engineering Team for identification products with NXP Semiconductors, where he has been a supporting customer in improving their RFID antenna design as well as in EMC and EMI optimization. He Joined Silicon Austria Labs in 2019 as a Senior Research Engineer to further work on coexistence and electromagnetic compatibility.

Bernhard Auinger (Member, IEEE) received the master's degree (Dipl.-Ing.) in electrical engineering and the Dr.techn. degree (with Distinction) from the Graz University of Technology, Graz, Austria, in 2004 and 2015, respectively. From 2015 to 2018, he was with Electromagnetic Compatibility for Power Electronics and the Preestimation of EMC. From 2011 to 2015, he was involved in theoretical investigations for wireless communications test procedures of LTE handsets using MIMO, which was a cooperation between the Institute of Microwave and Photonic Engineering, Graz University of Technology, and the company Rohde & Schwarz, Munich, Germany. From 2005 to 2011, he initiated and led the electromagnetic compatibility group for automotive ICs with Philips Semiconductors and NXP Semiconductors. During his studies, he was engaged in the comet mission ROMAP/ROSETTA of the European Space Agency. He is currently leading the EMC Department, Silicon Austria Labs, Graz, where he aims for a paradigm shift in electronics design by enabling the simulation of electromagnetic compatibility of electronic-based systems.

Wolfgang Bösch (Fellow, IEEE) received the Dipl.-Ing. degree from the Technical University of Vienna, Vienna, Austria, in 1985, the Ph.D. degree from the Graz University of Technology, Graz, Austria, in 1988, and the M.B.A. degree from the School of Management, University of Bradford, Bradford, U.K., in 2004. In 2010, he joined the Graz University of Technology to establish the Institute for Microwave and Photonic Engineering. For the last eight years, he has been the Dean of the Faculty of Electrical and Information Engineering, which currently incorporates 13 institutes and 20 full professors covering the areas of energy generation and distribution, electronics, and information engineering. He is responsible for the faculty's strategic development, budget, and personnel. Before this, he was a Chief Technology Officer (CTO) with the Advanced Digital Institute, Shipley, U.K. He was also the Director of the Business and Technology Integration, RFMD, Newton Aycliffe, U.K. For almost ten years, he was with Filtronic plc, Leeds, U.K., as the CTO of Filtronic Integrated Products and the Director of the Global Technology Group. Before joining Filtronic, he held positions with the European Space Agency, Noordwijk, The Netherlands, working on amplifier linearization techniques; with MPR-Teltech, Burnaby, BC, Canada, working on monolithic microwave integrated circuit technology projects; and with the Corporate Research and Development Group, M/A-COM, Boston, MA, USA, where he worked on advanced topologies for high-efficiency power amplifiers. He was with DaimlerChrysler Aerospace (currently, Hensoldt), Ulm, Germany, for four years, working on T/R modules for airborne radar. He has published more than 180 articles and holds four patents. He is a Fellow of the Institution of Engineering and Technology.

Jasmin Grosinger (Senior Member, IEEE) is an Associate Professor with the Institute of Microwave and Photonic Engineering, Graz University of Technology, Austria. Her research is focused on sustainable wireless electronics and systems. She also works as a Visiting Associate Professor with the Graduate School of Engineering, Tohoku University, Japan. She has co-authored several peer-reviewed publications, book chapters, and invention disclosures. For her Ph.D. work, she received the First Prize from the Industrial Union of the Austrian Automotive Industry's Jubilee Foundation. In 2021, she received the Mind the Gap—Diversity Award from the Graz University of Technology. Since 2019, she has been serving as an Associate Editor for the IEEE MICROWAVE AND TECHNOLOGY LETTERS. Since 2023, she has chaired the Wireless Power Technologies (WPT) Journal Exploration Working Group (IEEE WPT Initiative). She is a member of the IEEE Microwave Theory and Technology Society (MTT-S) Technical Committees 25 (Wireless Power Transfer and Energy Conversion) and 26 (RFID, Wireless Sensors, and IoT). She has been recognized as a Distinguished Microwave Lecturer of MTT-S and is an Elected Voting Member of its Administrative Committee, chairing the Meetings and Symposia Committee in 2024.